Hole Trapping at Hydrogenic Defects in Amorphous Silicon Dioxide

Al-Moatasem El-Sayed[a], Matthew B. Watkins[a], Tibor Grasser[b], Valeri V. Afanas'ev[c], Alexander L. Shluger[a]

[a]*Department of Physics and Astronomy and London Centre for Nanotechnology, University College London, Gower Street, London, WC1E 6BT, United Kingdom*
[b]*Institute for Microelectronics, Technische Universität Wien, A-1040, Vienna, Austria*
[c]*Department of Physics, University of Leuven, Celestijnenlaan 200D, 3001 Leuven, Belgium*

Abstract

We used *ab initio* calculations to investigate the hole trapping reactions at a neutral defect center generated in amorphous silicon dioxide networks by the interaction of strained Si–O bonds with atomic hydrogen, a so-called hydroxyl E′ center. It was found that the hole trapping at this defect leads to two distinct charged configurations. The first one consists of an H atom bound to a bridging O in a hydronium-like configuration. The second configuration involves relaxation of a Si atom through the plane of its oxygen neighbors facilitated by a weak interaction with a 2-coordinated O atom. The distribution of total energy differences between these two configurations calculated for a number of amorphous network models has a width of about 1.0 eV. These hole trapping reactions are discussed in the context of Si complementary metal-oxide-semiconductor device reliability issues.

Keywords: Hydroxyl E′ centre, SiO_2 point defects, Device Reliability, DFT, Positively charged E′

1. Introduction

After being at the core of the development of the semiconductor industry for more than 50 years, SiO_2 based dielectrics are still used in nearly all integrated circuits as tunnel, gate, field, or interconnect insulating layers. A common feature of these materials is their amorphous structure. The disorder inherent to these materials enables the reduction of strain caused by the mismatch between the insulating layer and other materials thanks to the structural flexibility of the oxide network. In particular, at the interfaces with semiconductors a reduced mismatch allows for a lower interface defect density leading to improved device performance. However, on the flip side, the flexibility of the amorphous oxide network is associated with a high concentration of strained bonding configurations which, being energetically less favorable than regular bonds, may lead to network instabilities and generation of electrically active defects.

In particular, the reactivity of strained Si–O bonds in a-SiO_2 with atomic hydrogen has been the subject of a number of studies. When released into the oxide by exciting H-containing bonds using ArF or F_2 lasers [1, 2], atomic hydrogen was found to diffuse easily through the silica network with activation energies of 0.1–0.2 eV. However, a number of H-related defects were also detected using electron spin resonance after the excitation [3–6].

In particular, a 0.08 mT doublet due to proton hyperfine splitting was assigned to a Si dangling bond coordinated by two bridging oxygens and an OH group. This center is thought to result from the interaction of H^0 with electronically excited strained Si–O bonds [5].

Recent *ab initio* calculations demonstrated that atomic H can break strained Si–O bonds in the a-SiO_2 network generating a new defect called the hydroxyl E′ center [7]. In this defect, a dangling bond on a 3-coordinated Si faces a hydroxyl group (see Fig. 1a). The energy barrier for formation of this defect with respect to an interstitial H atom was found to be > 0.5 eV. An unpaired electron is strongly localized on the 3-coordinated Si with a single-electron level positioned at $\approx$ 3 eV above the oxide valence band (VB), i.e., slightly below the VB top of silicon at the Si/SiO_2 interface in metal-oxide-semiconductor (MOS) devices. The neutral hydroxyl E′ center has a second configuration whereby the 3-coordinated Si displaces through the plane of its oxygen neighbors to form a back-projected configuration which is shown in Fig. 1b. This movement of the Si atom requires overcoming a barrier of about 1.8 eV and the resulting configuration is on average about 0.7 eV higher in energy than the one shown in Fig. 1a.

The position of the defect level and its high degree of localization suggest that in Si MOS devices holes can be trapped by the hydroxyl E′ center in the amorphous oxide layer under negative bias application. Therefore, this defect can take part in hole trapping/de-trapping processes and is a potential candidate for a defect responsible for negative bias temperature instability (NBTI) [8]. Here we demonstrate that upon hole trapping the hydroxyl E′
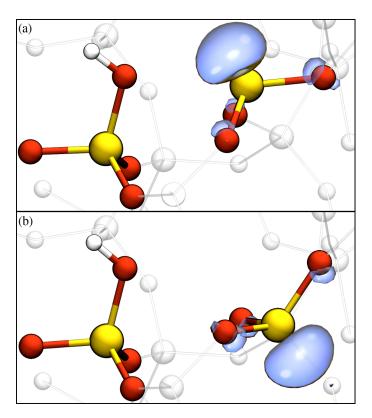
Figure 1: The atomic structure and spin density of the forward- and back-projected configurations of the hydroxyl E′ center in the neutral charge state. The larger yellow balls are Si, the medium sized red balls are O, and the small white ball is H. The transparent, blue polyhedron is the spin density of the defect. The smaller, colorless balls and sticks in the background of the figure are the remaining atoms in the amorphous oxide network. a) The forward-projected configuration of the defect consists of a 3-coordinated Si facing a hydroxyl group. b) The back-projected configuration of the defect consists of a 3-coordinated Si facing away from the hydroxyl group. Both spin densities are plotted with an isovalue of 0.02. The plots indicate that the spin density is highly localized on the defect center.

Figure 2: The atomic structure and the lowest unoccupied electronic state of the positively charged hydroxyl E′ center. The color scheme is the same as that in figure 1. However, transparent, green polyhedra depict the lowest unoccupied molecular orbital (LUMO) of the system hosting the hole. a) The protonic configuration: an Si–O bond reforms and an H atom is now bound to a bridging O. b) The back-projected configuration: the 3-coordinated Si has relaxed through the plane of its O neighbors and interacts weakly with a 2-coordinated O. The unoccupied states in both configurations are plotted with an isovalue of 0.07. The LUMO in both configurations is highly localized on the defect center.

center may take two distinct atomic configurations with a broad distribution of barrier heights between the two states. This makes it relevant for the NBTI analysis based on bi-stable hole trapping defects in CMOS devices [9, 10].

2. Methods of Calculations

To obtain a distribution of the defect's properties, the ReaxFF force-field [11, 12], implemented in the LAMMPS code [13], was used to generate 86 periodic models of a-SiO$_2$, each containing 216 atoms. Starting from a crystalline polymorph of SiO$_2$, classical molecular dynamics and a melt and quench procedure was used to obtain the amorphous structures. This procedure is described in detail in previous publications [7, 14].

Density functional theory (DFT), implemented in the CP2K code [15], was then used to further optimize the geometries of amorphous structures and calculate their electronic structures. The non-local functional PBE0_TC_LRC was used in all calculations with a cutoff
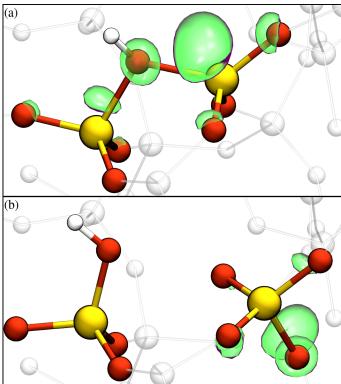
radius of 2.0 Å for the truncated Coulomb operator [16]. Inclusion of Hartree-Fock exchange provides an accurate description of the band gap and localized states that may be involved in charge trapping processes. Calculations of the hole trapping configurations were obtained by removing an electron and adding a uniform background negative charge. The CP2K code uses a Gaussian basis set with an auxiliary plane-wave basis set [17]. A double-ζ basis set with polarization functions [18] was used for all atoms in conjunction with the Goedecker-Teter-Hutter (GTH) pseudopotential [19]. The cut-off for the auxiliary plane wave basis was set to 5440 eV (400 Ry). To reduce the computational cost of non-local functional calculations, the auxiliary density matrix method (ADMM) was employed [20]. The electron density is mapped onto a much sparser Gaussian basis set containing less diffuse and fewer primitive Gaussian functions than the one employed in the rest of the calculation. All geometry optimizations were performed using the Broyden-Fletcher-Goldfarb-Shanno (BFGS) optimizer to minimize forces on atoms to within 37 pN (2.3 $\times 10^{-2}$ eV Å^{-1}) in periodic

cells with fixed cell vectors. Barriers between configurations were calculated using the climbing image nudged elastic band method (CI-NEB) [21]. Linear interpolation was used to generate 10 images for a band which was to be optimized, with each of the images connected by a spring with a force constant of 2 eV $Å^2$.

The structural properties of the models obtained using this procedure show excellent agreement with previous theoretical studies and experiment. The average density of the a-SiO$_2$ samples obtained were 2.16 g cm^{-3}, ranging from 1.99 to 2.27 g cm^{-3}. The distribution of Si–O bond lengths is a Gaussian centered around 1.62 Å. Similarly, the Si–O–Si and O–Si–O angles are also Gaussian distributed, centered around 146° and 109°, respectively. The neutron structure factors calculated for our models show excellent agreement with the experiment [22]. The agreement extends to high Q values, indicating that our models describe both the short- and long-range order and are indeed representative of a-SiO$_2$.

3. Hole Trapping at the Hydroxyl E′ center

Single neutral hydroxyl E′ centers were optimized in 86 independent models of a-SiO$_2$. A hole was then added to each system and the total energy of the system was minimized with respect to its atomic coordinates. This resulted in two distinct defect configurations described below.

3.1. Protonic Configuration

To begin with, a total of 61 structures with a hole traped at the hydroxyl E′ center were optimized. In the first hole trapped configuration a weak Si–O bond reforms at the 3-coordinated Si involving a large displacement of an O atom toward the Si. This results in a hydronium-like structure, where a proton is bound to a bridging O making it 3-coordinated while the Si is now 4-coordinated, as seen in Fig. 2a. The LUMO of this configuration is also plotted in Fig. 2a and is clearly highly localized at the defect center. This configuration is similar to the one suggested by DeNijs *et al.* [23] and will be referred to as the protonic configuration herein. From the 61 initial structures, a total of 59 spontaneously form the protonic configuration upon the hole trapping, indicating its natural abundancy. The O–H bonds display a narrow distribution, averaging at 0.98 Å and ranging from 0.97 to 1.05 Å. The Si–O bonds associated with the bridging O are longer than the typical Si–O bond in a-SiO$_2$, averaging at 1.84 Å and ranging from 1.79 to 1.94 Å. The average Mulliken charge of the H atom in this configuration is 0.31 $|e|$, slightly more positive than the H in the neutral hydroxyl E′ center, which has an average Mulliken charge of 0.24 $|e|$. Removal of the electron from the 3-coordinated Si atom leads to a localized unoccupied state which sits 1.2 eV on average below the a-SiO$_2$ conduction band (CB), ranging from 1.0 eV to 3.2 eV below the a-SiO$_2$CB.

3.2. Back-projected Configuration

The second configuration closely resembles the back-projected configuration of the E′ center in a-SiO$_2$ [24, 25]. We found that the 3-coordinated Si of the neutral hydroxyl E′ center can relax through the plane of its O neighbors in order to interact with a 2-coordinated O, as can be seen in Fig. 2b. From the initial 61 structures, only 2 spontaneously formed the back-projected configuration. However, a geometrical fingerprint was identified which allowed us to reliably generate more puckered structures. In particular, we found that Si sites which have long Si–O bonds (> 1.65 Å) and which, when inverted through the plane of its neighbors, are located within 1.9 Å from a 2-coordinated O atom would reliably generate back-projected configurations. In our models, we estimate that Si sites which satisfy these criteria amount to $\approx 1\%$ of total Si sites. In total, we have studied 25 back-projected configurations.

The atomic structure of the back-projected configuration is characterized by a hydroxyl group facing a 3-coordinated Si which has inverted through the plane of its O neighbors [see Fig. 2b]. The LUMO in this configuration is also plotted in Fig. 2b and, similar to the protonic configuration, is highly localized on the defect center. The distance between the hydroxyl group and the Si after it has inverted through the plane of its oxygen neighbors is on average 3.15 Å, ranging from 2.92 to 3.38 Å. The inverted Si has 3 strong Si–O bonds which average at 1.59 Å, ranging from 1.56 Å to 1.65 Å. These bonds are shorter than the typical Si–O bond in a-SiO$_2$, which averages at 1.62 Å. The Si also has a long range interaction with the O toward which it has puckered, with the distance between the inverted Si and the bridging O averaging at 1.83 Å and ranging from 1.74 Å to 1.90 Å. The distance between the inverted Si and the O is, however, much longer than an average Si–O bond, indicating a weak interaction between this Si and O. The hole is trapped in a localized LUMO state positioned on average 1.3 eV below the bottom of the SiO$_2$ CB and is predominantly localized on the Si atom [see Fig. 2b], i.e., in a similar position to the protonic configuration and also does not have any occupied states in the band gap.

Importantly, the electron trapping in the back-projected configuration of the hole trap (Fig. 2b) leads to the formation of the back-projected configuration of the neutral hydroxyl E′ center shown in Fig. 1b, closing the hole trapping/de-trapping cycle.

3.3. Thermodynamics and Kinetics of the Hydroxyl E′ Center's Hole Traps

Interestingly, the relative stabilities of the protonic and back-projected configurations are not qualitatively the same. We find that the total energy difference between the puckered configuration and the protonic configuration vary over a 1.15 eV energy range, with the puckered configuration ranging from being by 0.44 eV more to 0.71 eV

less stable. There is no clear correlation between the total energy differences and the geometrical parameters of the different centers, such as Si–O bond lengths and angles.

The major difference in atomic structure between the protonic and back-projected configurations is a relaxation of a Si through the plane of its 3 O neighbors. We have calculated the barriers between the protonic configurations and the puckered configurations using a Nudget Elastic Band method. A corresponding band was initially set up by interpolating 10 images between the two configurations and this band was then optimized using CI-NEB. Similar to the total energy differences between two configurations, we find that the barriers also show qualitatively different behavior. The barrier from the protonic configuration to the back-projected configuration ranges from negligibly small (i.e., less than 0.05 eV) to 0.91 eV, while the barrier for the reverse transformation (i.e., the back-projected to the protonic configuration) ranges from 0.0 to a maximum of 0.76 eV. The trajectory of the barrier from the protonic configuration to the puckered configuration does not deviate much from the initial band interpolation, with the motion remaining a movement of an Si atom through the center of the plane of its neighbors, breaking an Si–O bond in the process and forming a weak Si–O interaction with a bridging oxygen (see Fig. 2).

4. Discussion and Conclusions

Reliability issues in electronic devices have implicated charge trapping defects in the oxide. In particular, NBTI is probably caused by bi-stable hole trapping defects; that is, defects which have a ground and metastable state in both the neutral and positively charged states [9, 10]. Although previous studies have focused on conventional defects in SiO_2, such as the neutral O vacancy and the E'_γ center [26], there is evidence that hydrogen complexed defects may be involved too, as the detrimental effects of NBTI increase when devices are processed in a hydrogen environment [27]. In this paper, we have shown that a neutral, hydrogen complexed defect, the hydroxyl E' center, can trap holes and exhibits a bi-stability in both the neutral and positive charge states with a forward- and a back-projected configuration shown in Figs. 1 and 2 (see also ref. [7]). Therefore the hydroxyl E' center has a number of characteristics that could implicate it in contributing to electronic device reliability issues.

The calculations [7] demonstrate that there are two potential paths to creating the hydroxyl E' center. The first involves the direct reaction of atomic H with strained Si–O bonds and requires overcoming a barrier of ≈ 1 eV at a precursor site to generate this defect. This barrier is rather high compared to the diffusion barrier for atomic H, which is about 0.1 eV [2]. This defect can, however, be easily passivated in the excess of atomic H [7]. Our calculations also show that if molecular hydrogen can overcome a barrier of 1.74 eV it can generate the same passivated configuration of the hydroxyl E'. Although this may seem like a rather

high barrier, there is experimental evidence that the concentrations of both Si–H and O–H bonds increase after anneals in H_2 and/or forming gas [28, 29]. These anneals are common device processing techniques and seem to increase the amount of Si–H bonds in the device. Our calculations also demonstrate that the barrier to de-passivating this defect in the presence of atomic H is only 0.20 eV. This is the second mechanism of creating the hydroxyl E' center: if atomic H is released during device operation then the hydroxyl E' defect may be activated via de-passivating Si-H bonds and formation of H_2 molecules [7]. Once the defect becomes active, it may trap a hole as described in the present work.

5. Acknowledgments

References

[1] K. Kajihara, L. Skuja, M. Hirano, H. Hosono, Phys. Rev. B 74 (2006) 094202.
[2] K. Kajihara, L. Skuja, M. Hirano, H. Hosono, Phys. Rev. Lett. 89 (2002) 135507.
[3] J. Vitko, J. Appl. Phys. 49 (1978) 5530.
[4] V. A. Radzig, Kinet. Katal. 20 (1979) 456.
[5] L. Skuja, K. Kajihara, M. Hirano, A. Saitoh, H. Hosono, J. Non-Cryst. Solids 352 (2006) 2297–2302.
[6] L. Skuja, K. Kajihara, M. Hirano, H. Hosono, Nucl. Instrum. Methods Phys. Res. B 266 (2008) 2971–2975.
[7] A.-M. El-Sayed, M. B. Watkins, T. Grasser, V. V. Afanas'ev, A. L. Shluger, Phys. Rev. Lett. 114 (2015) 115503.
[8] T. Grasser (Ed.), Bias Temperature Instability for Devices and Circuits, Springer.
[9] T. Grasser, Microelectron. Reliab. 52 (2012) 39–70.
[10] T. Grasser, B. Kaczer, W. Goes, H. Reisinger, T. Aichinger, P. Hehenberger, P. J. Wagner, F. Schanovsky, J. Franco, M. T. Luque, M. Nelhiebel, IEEE Trans. Electron Dev. 58 (2011) 3652–3666.
[11] A. C. T. van Duin, A. Strachan, S. Stewman, Q. Zhang, X. Xu, W. Goddard, J. Phys. Chem. A 107 (2003) 3803–3811.
[12] J. C. Fogarty, H. M. Aktulga, A. Y. Grama, A. C. T. van Duin, S. A. Pandit, J. Chem. Phys. 132 (2010) 174704.
[13] S. Plimpton, J. Comp. Phys. 117 (1995) 1–19.
[14] A.-M. El-Sayed, M. B. Watkins, V. V. Afanas'ev, A. L. Shluger, Phys. Rev. B 89 (2014) 125201.
[15] J. VandeVondele, M. Krack, F. Mohamed, M. Parrinelo, T. Chassaing, J. Hutter, Comp. Phys. Comm. 167 (2005) 103.
[16] M. Guidon, J. Hutter, J. VandeVondele, J. Chem. Theory Comput. 5 (2009) 3013–3021.
[17] G. Lippert, J. Hutter, M. Parrinello, Mol. Phys. 92 (1997) 477–487.
[18] J. VandeVondele, J. Hutter, J. Chem. Phys. 127 (2007) 114105.

[19] S. Goedecker, M. Teter, J. Hutter, Phys. Rev. B 54 (1996) 1703–1710.

[20] M. Guidon, J. Hutter, J. VandeVondele, J. Chem. Theory Comput. 8 (2010) 2348–2364.

[21] G. Henkelman, B. P. Uberuaga, H. Jnsson, J. Chem. Phys. 113 (2000) 9901–9904.

[22] S. Susman, K. J. Volin, D. L. Price, M. Grimsditch, J. P. Ringo, R. K. Kalia, P. Vashishta, G. Gwanmesia, Y. Wang, R. C. Liebermann, Phys. Rev. B 43 (1991) 1194.

[23] J. de Nijs, K. Druijf, V. Afanas'ev, E. van der Drift, P. Balk, Appl.Phys.Lett. 65 (1994) 2428–2430.

[24] D. Griscom, M. Cook, J. Non-Cryst. Solids 182 (1995) 119 – 134.

[25] A. Kimmel, P. Sushko, A. Shluger, G. Bersuker, in: R. Sah, J. Zhang, Y. Kamakura, M. Deen, J. Yota (Eds.), Silicon Nitride, Silicon Dioxide, and Emerging Dielectrics 10, volume 19, ECS Transactions, 2009, pp. 2–17.

[26] F. Schanovsky, W. Gös, T. Grasser, J. Comput. Electron. 9 (2009) 135–140.

[27] G. Pobegen, T. Aichinger, M. Nelhiebel, Impact of Hydrogen on the Bias Temperature Instability, Springer, pp. 485–506.

[28] J. A. Theil, D. V. Tsu, M. W. Watkins, S. S. Kim, G. Lucovsky, J. Vac. Sci. Technol. A 8 (1990) 1374–1381.

[29] G. Lucovsky, Solid State Commun. 29 (1979) 571 – 576.